NANO LETTERS

2008
Vol. 8, No. 5
1341-1346

Optical Antenna Effect in Semiconducting Nanowires

G. Chen,[†,‡,§] Jian Wu,[†,§] Qiujie Lu,[§] H. R. Gutierrez,[§] Qihua Xiong,[§,||,⊥] M. E. Pellen,[#] J. S. Petko,[#] D. H. Werner,[#] and P. C. Eklund*[,§,⊥]

Department of Physics, Department of Materials Science and Engineering, and Department of Electrical Engineering, The Pennsylvania State University, University Park, Pennsylvania 16802

Received January 2, 2008; Revised Manuscript Received February 14, 2008

ABSTRACT

We report on investigations of the interaction of light with nanoscale antennae made from crystalline GaP nanowires (NWs). Using Raman scattering, we have observed strong optical antenna effects which we identify with internal standing wave photon modes of the wire. The antenna effects were probed in individual NWs whose diameters are in the range 40 < *d* < 300 nm. The data and our calculations show that the nature of the backscattered light is critically dependent on the interplay between a photon confinement effect and bulk Raman scattering. At small diameter, *d* < 65 nm, the NWs are found to act like a nearly perfect dipole antenna and the bulk Raman selection rules are masked leading to a polarized scattering intensity function $I_R \sim \cos^4 \theta$. Underscoring the importance of this work is the realization that a fundamental understanding of the "optical antenna effect" in semiconducting NWs is essential to the analysis of all electro-optic effects in small diameter filaments.

An intriguing application of quasi-one-dimensional nanofilaments, such as single-walled carbon nanotubes (SWNTs) or semiconducting nanowires (SNWs), would be their use as nanoscale antennas.[1] The simplest antenna is a linear structure. It receives and transmits polarized electromagnetic (EM) radiation with a $\cos^2 \theta$ or dipolar dependence, where θ is the angle between the antenna axis and the incident or radiated electric field.[2] When the length of the classical antenna matches a multiple of the half-wavelength of the EM field, it is said to "resonate", and radiation is most easily received and radiated. The optical antenna effect we report here via Raman scattering studies should have nothing to do with phonon or electron confinement within the waist of the NW. Instead, we propose that the Raman effects that we observe are a manifestation of *photon* confinement in the NW. For example, for our smallest diameter NWs, the backscattered Raman intensity vs θ is observed to exhibit a $\sim\cos^4 \theta$ response, independent of the nature of the vibration (phonon) participating in the Raman scattering. However, as the NW diameter increases, more complex polar scattering patterns emerge that we ascribe to the interplay between the ability of the incident EM wave to set up an internal field in the wire and the natural polarization dependence of the Raman scattering tensor.

An antenna effect in SWNTs was first predicted by Ajiki and Ando.[3] From calculating the electric dipole matrix elements for this molecular wire, they predicted that the optical absorption is strongly suppressed when the incident electric field is perpendicular to the nanotube axis. This is a manifestation of the symmetry of the electronic wave function in the nanotube. Indeed, a "Raman antenna effect" was first reported by Duesberg[4] et al. in resonant scattering from SWNTs where it was observed that the Raman backscattering intensity from both radial and tangential nanotube phonons both exhibited a classic $\cos^2 \theta$ dependence, i.e., a dipole pattern, in apparent contradiction with expectations based on group theory for nonresonant scattering.[4,5] A more complicated multipolar antenna effect was also observed in Raman scattering in SWNTs.[6] Recently, an array of multiwalled carbon nanotubes (MWNTs) on a substrate has demonstrated the ability to absorb light as an antenna when the length of the MWNTs in the array matches the wavelength of the light.[7] Strongly polarized Raman scattering has also been observed in WS_2 nanotubes, but no theory for this observation or a connection with a NW antenna effect has been made.[8] It is not until recently that Raman scattering from individual NWs of GaN[9,10] and SiC[11] have been shown to exhibit a strong dependence on the polarization angle between the incident electric field and the NW axis. In the

* To whom all correspondence should be addressed: Email: pce3@psu.edu.
† These authors contributed equally to this work.
‡ Present address: Honda Research Institute USA, Inc., 1381 Kinnear Rd., Suite 116, Columbus, OH 43212.
§ Department of Physics.
|| Present address: Department of Chemistry and Chemical Biology, Harvard University, 12 Oxford Street, Cambridge, MA 02138.
⊥ Department of Materials Science and Engineering.
Department of Electrical Engineering.

10.1021/nl080007v CCC: $40.75
Published on Web 04/19/2008

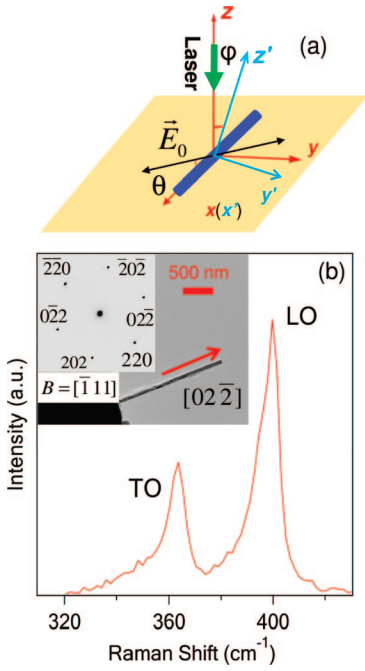

Figure 1. (a) Backscattering geometry used for polarized Raman experiments on individual GaP NWs. The incident electric field is polarized at an angle θ with respect to the NW axis. (b) Typical polarized Raman scattering spectrum ($\theta = 0°$) for the GaP NW shown in the accompanying TEM image as protruding over a hole in the TEM grid. The SAD pattern (inset) shows the wire grew along ⟨110⟩.

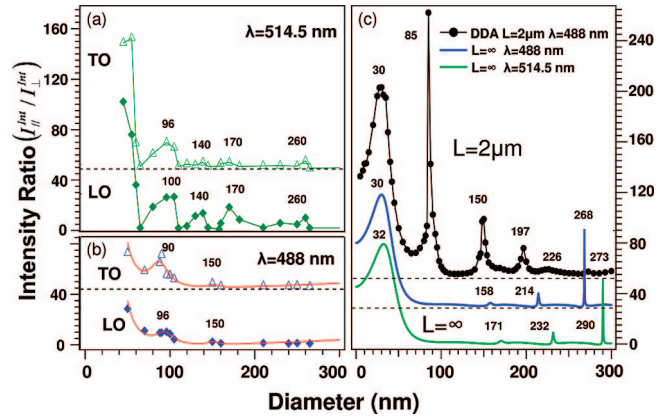

Figure 2. GaP NW diameter (d) dependence of the EM field intensity ratios ($I_{||}/I_{\perp}$), where || and ⊥ refer to the direction of the electric field relative to the NW axis. (a) and (b) Integrated Raman backscattering ratio ($I_{||}^{R}/I_{\perp}^{R}$) for both LO and TO scattering: (a) 514.5 nm and (b) 488 nm excitation. (c) Calculated d dependence of the *internal* EM intensity ratio ($I_{||}^{Int}/I_{\perp}^{Int}$). (top) $L = 2$ μm NW with 488 nm excitation. $L = \infty$ NW with 488 nm excitation (middle) and 514.5 nm radiation (bottom). (Numbers above the peaks refer to the diameter at the resonance in nanometers.)

case of SiC NWs, it was proposed that a "shape resonance" should be taken into account to explain the results.[11]

The GaP NWs studied here were grown by the pulsed laser vaporization (PLV) of a $(GaP)_{0.95}Au_{0.05}$ target in argon gas. The NWs grew from small gold particles entrained in the Ar flowing down a heated quartz reactor tube centered in a tube furnace.[12] Detailed information about our growth conditions for PLV-GaP and our characterization procedures have been published.[12,13] Transmission electron microscopy (TEM) (lattice images and selected area diffraction (SAD) patterns) show that most, if not all, of the GaP NWs grown in our PLV system are crystalline. They exhibit the cubic zinc blende structure. From TEM observations, the ⟨110⟩ growth direction seems to be slightly preferred, but several other growth directions are also observed, e.g., ⟨111⟩. Isolated GaP NWs were prepared for Raman scattering studies by dispersing them in ethanol using mild ultrasound and either immediately depositing a drop of this suspension onto a Si substrate with lithographic markers to define the NW position or by depositing the NW directly onto TEM grids. Atomic force microscopy (AFM) or TEM was then used to measure the diameter of the NWs. Due to fluctuations in the NW diameter along its length, we estimated that the diameter d is accurate to ±1.5 nm.

In Figure 1a, we display the geometry used to observe the optical antenna effects using a Raman microscope (Renishaw, INVIA or JY, T64000). The coordinate system x', y', z' (blue) is fixed to an orthogonal set of crystal directions of the NW. The x,y,z system (red) represents the "lab" axes that define the electric field polarization and propagation for the incident and scattered light. Light from a laser is incident along the $-z$ direction onto the NW lying along the x axis. Using a half-wave plate placed above the 100× objective lens,[4,9] the incident electric field $\vec{E}_i$ from the laser was polarized at an angle θ with respect to the NW axis and the backscattered light was collected along the z direction. Using a polarization analyzer, we collected Raman spectra with the scattered electric field $\vec{E}_s \parallel \vec{E}_i$ for low laser power ($P < 2$ mW). The experiments were conducted under ambient conditions.

In Figure 1b, we display a typical polarized Raman spectrum for an individual GaP NW ($d = 80$ nm) showing two peaks due to longitudinal optic (LO) and transverse optic (TO) phonon scattering. The data were collected as shown in Figure 1a (backscattering) using 514.5 nm excitation and for polarization angle $\theta = 0°$. Raman bands are observed at 363 cm^{-1} (TO) and 400 cm^{-1} (LO), in good agreement with first-order scattering from bulk crystalline GaP.[14] In some of our GaP NWs, a weaker Raman band may appear on the lower frequency side of the LO phonon peak. This is due to scattering from surface optical (SO) modes activated by surface roughness and/or faceting on the NW surface.[13,15] The inset to Figure 1b shows a low magnification TEM image of an individual GaP NW protruding over a hole in a TEM grid with a SAD pattern indicating that this particular NW grew along direction ⟨110⟩. If the wires were deposited on a Si wafer, the growth direction for the individual wires could not be confirmed by SAD, although ⟨110⟩ and ⟨111⟩ are the prevalent growth directions. AFM z-scan was then used to determine the NW diameter.

In the left-hand panels in Figure 2, we plot experimental results for the *ratio* of the integrated Raman band intensity ($I_{||}^{X}/I_{\perp}^{X}$) vs the NW diameter (d), where X refers to LO(TO) phonons that are participating. The symbols || and ⊥ refer, respectively, to polarization $\theta = 0°$ and 90°; cf. Figure 1a. The Raman intensity data shown in these panels were all

collected from NWs of known diameter (AFM z-scan) lying on a Si(100) substrate with a 200 nm oxide. Data in Figure 2a were obtained using 514.5 nm excitation and a Renishaw INVIA microRaman spectrometer, and data in Figure 2b were obtained using 488 nm excitation and a Jobin-Yvon T64000 microRaman spectrometer. For clarity, the TO data in each case have been displaced vertically. Notice that the smallest diameter wires studied, i.e., $d \sim 50$ nm, exhibit a very large anisotropy in the scattering, i.e., the intensity ratio $(I_{||}^{X}/I_{\perp}^{X}) \sim 30$ for 488 nm excitation and $\sim$100 for 514.5 nm excitation. These small diameter wires therefore appear to act like a classical dipole antenna; i.e., they are essentially responding only to radiation polarized parallel to the antenna (NW) axis. This antenna behavior is observed for both LO and TO phonon Raman scattering in very small diameter NWs.

In the right panel of Figure 2, i.e., Figure 2c, we plot the *calculated* volume-averaged *internal* electromagnetic (EM) field intensity ratio of the NW, i.e., $(I_{||}^{Int}/I_{\perp}^{Int})$ vs the NW diameter d. The calculations are made for 488 nm light incident at right angles to the NW axis with $\vec{E}$ polarized either || or $\perp$ to the wire axis. Results are shown for infinitely long wires ($L = \infty$) and also for finite length wires ($L = 2\ \mu$m). Since the GaP crystal lattice is cubic, the electric susceptibility tensor is a scalar, and information on the orientation of the NW crystal axes relative to the incident electric field is not needed in these calculations. The solution for scattering from infinitely long wires ($L = \infty$) was first published by Lord Rayleigh in 1918[16] who expanded the incident, scattered, and internal electric fields in terms of Bessel functions of the first kind and order n. His derivation has been re-examined several times in the literature.[2,17,18] Lossless solutions to this $L = \infty$ problem have been used recently to explain the Raman scattering from Si nanocones.[19] For short wires $L = 1$ and 2 μm, we have used a numerical approach based on the discrete-dipole approximation (DDA).[20,21] DDA is a software package which allows us to calculate scattering and absorption of EM waves numerically from targets (particles) with arbitrary geometries. By dividing the target (particle) into small cubes and replacing each cube with a point dipole at its center consistent with the dielectric function of the macroscopic material, the interaction between incident EM plane wave and the target can be solved very accurately.[21] The DDA code can be used to calculate the EM scattering in any direction, the effective extinction of the incident beam as well as the internal and surface electric or magnetic fields that are the response to the incident wave. It should be pointed out that the calculations on short wires were made with the entire NW illuminated by an infinitely wide plane wave. However, in the experiments, the incident light was focused onto a $\sim$1 μm spot on a much longer wire ($\sim$20 μm), i.e., the NW was under-illuminated by a converging beam.

It is interesting to compare the results for infinite ($L = \infty$) and short ($L = 2\ \mu$m) GaP NWs (Figure 2c). For $L = \infty$, results are displayed for light incident both at 488 nm (blue curve) and 514.5 nm (green curve). For $L = 2\ \mu$m, only results for 488 nm excitation have been made and are shown.

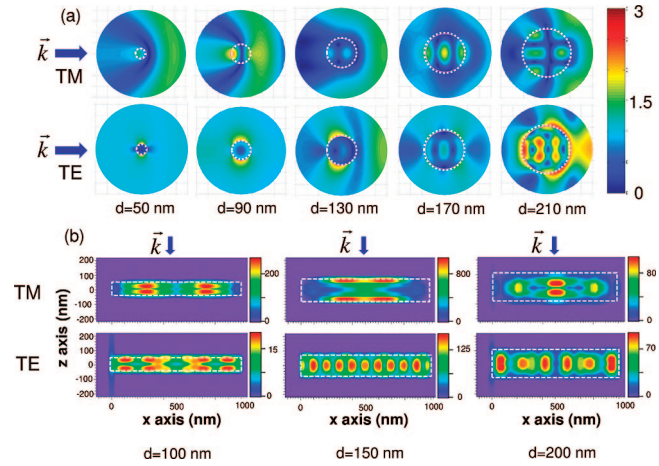

Figure 3. Calculated internal electric field *amplitude* maps (488 nm) for GaP NWs with color-coded scale appearing to the right. TM and TE refer, respectively, to transverse magnetic ($\theta = 0°$) and transverse electric ($\theta = 90°$) excitation with the light incident at right angles to the NW axis. (a) results for the radial cross section of $L = \infty$ NWs. (b) Results for the axial cross section of $L = 2\ \mu$m NWs.

From the figure, it can be seen that analytical and DDA calculations predict a similarly placed, lowest order (broad) resonance centered at $d \sim 30$ nm. The infinite wire ($L = \infty$) calculations predict three more higher-order resonances in the range $150 < d < 300$ nm. These additional resonances are significantly narrower than the fundamental resonance. As shown for $L = \infty$ wires, the peaks or resonances in the calculated internal electric field intensity ratio shift noticeably with the incident wavelength. This is a simple consequence of the fact that the classical EM theory of scattering depends on the variable nx/λ, where x is a physical dimension of the scattering object (diameter or length or both) and n is the real part of the complex refractive index $n^* = n + ik$.[18,22] For $L = 2\ \mu$m NWs with $d < 300$ nm, our DDA calculations predict six resonances altogether, i.e., two more than predicted for infinite wires. This is the case because the resonances in short wires will depend not only on the NW d but also on the length L. The more numerous resonances in $(I_{||}^{Int}/I_{\perp}^{Int})$ for the $L = 2\ \mu$m wire therefore should correspond to EM standing wave patterns that are forced to fit both radially and longitudinally into the NW.

In Figure 3, for 488 nm light incident as in Figure 1a, we show the calculated electric field *amplitude* $|\vec{E}|$ set up inside the NW. The color-coded amplitude maps are a manifestation of volume antenna effects within the NW. In Figure 3a, we show the maps within the radial cross section of an infinite length GaP NW; results are shown for several diameters between $d = 50$ and $d = 210$ nm; the color scale is fixed. Light was taken to be incident (blue arrow) normal to the NW axis and polarized either || (TM) or $\perp$ (TE) to the NW axis. The usual notation, TM or TE, refers to either transverse magnetic field (TM) excitation or transverse electric field (TE) excitation relative to the NW axis. In Figure 3b, we display the TM and TE results for $|\vec{E}|$ calculated for an axial cross section of an $L = 1\ \mu$m wire (DDA) for $d = 100$, 150, 200 nm. The amplitude color scale in Figure 3b is variable to allow the patterns to be more easily observed. Finally,

one should notice that the position of the diameter-dependent resonances for the calculated internal field ratio ($I_{||}^{Int}/I_{\perp}^{Int}$) (Figure 2c) and the experimental Raman scattering intensity ratios ($I_{||}^{LO}/I_{\perp}^{LO}$) and ($I_{||}^{TO}/I_{\perp}^{TO}$) (Figure 2a) are correlated at small diameters where we have many experimental observations. The correlation between ($I_{||}^{X}/I_{\perp}^{X}$) X = LO, TO and ($I_{||}^{Int}/I_{\perp}^{Int}$) vs d suggests that photon confinement strongly impacts the polarized Raman scattering from NWs.

We next develop a model to connect photon confinement and Raman scattering in NWs. Out of the model comes the realization that a polar plot of the X = TO and X = LO Raman back scattering intensity $I_X(\theta)$ from an individual crystalline NW can provide detailed information on the diameter, the growth direction, and the complete orientation of the NW crystal axes relative to the plane of the substrate.

Suppose the incident (i) and Raman scattered (s) photons are plane waves each specified by the pair of vectors ($\vec{E},\vec{k}$), where $\vec{E} = E\hat{e}$ and $\vec{k}$ are the photon electric field and wavevector, respectively. The scattering geometry can then be summarized in the conventional notation popularized by Porto and co-workers in the early 1960s, i.e., $\vec{k}_i[\hat{e}_i,\hat{e}_s]\vec{k}_s$,[22] or specifically as $\vec{z}(\vec{x}\cos\theta + \vec{y}\sin\theta, \vec{x}\cos\theta + \vec{y}\sin\theta)\vec{z}$ using the laboratory coordinates (x,y,z) shown in red in Figure 1a. The Raman scattering intensity from a NW can be written as a simplified expression which incorporates the selection rules for the scattering process incorporating the crystal symmetry as well as the internal electric field intensity set up inside the NW by the incoming plane wave.[19,23–25]

$$I_s \approx \omega_i^4 |\hat{e}_i \cdot R \cdot \hat{e}_s|^2 Q_i^2 Q_s^2 I_i \qquad (1)$$

where ω_i and I_i are, respectively, the frequency and intensity of the incident laser beam, $|\hat{e}_i \cdot R \cdot \hat{e}_s|^2$ is the Raman scattering tensor, and Q_i and Q_s are dimensionless internal electric field enhancement factors that depend on the geometry of the scattering object.[24] The Q factors are the signature of photon confinement and depend on the polarization angle θ, photon frequency ω, and the NW dimensions (d, L). Since the Raman frequency shift ($\Delta\omega$) is small, we set $Q_i = Q_s \equiv Q$ and the enhancement factor in eq 1 is simply Q^4. We then use our calculated results (DDA) for the volume averaged internal electric field intensity to obtain a result for $Q^2 \sim \bar{I}_{int}(\theta,d,L)/I_i$. For simplicity, our model ignores the spatial dependence of the internal EM field. R is the same Raman tensor as used in bulk scattering for LO or TO scattering involving a phonon of wave vector $\vec{q} = 2\vec{k}_i$ (backscattering). It is helpful that the (3 × 3) Raman tensor for LO and TO scattering can be different in form. In this case (zinc blende structure), one can obtain independent information from the LO and TO polar scattering patterns.

In Figure 4a, we display the results (DDA) for the volume-averaged internal electric field intensity $\bar{I}_{int}$ vs polarization angle θ for an $L = 1$ μm GaP NW for eight diameters in the range 50–265 nm and for 514.5 nm incident radiation as shown in Figure 1a. We choose $L = 1$ μm to correspond to the spot size of the laser beam on the NW. These calculations are independent of the specific growth direction ⟨hkl⟩, as the first-order electric susceptibility tensor is a scalar for the cubic zinc blende structure. For a $d = 50$ nm, we obtain $\bar{I}_{int} \approx \cos^2\theta$, i.e., a simple dipolar response. For diameters $d =$ 80 and 120 nm, the responses $\bar{I}_{int}$ are nearly dipolar, indicating

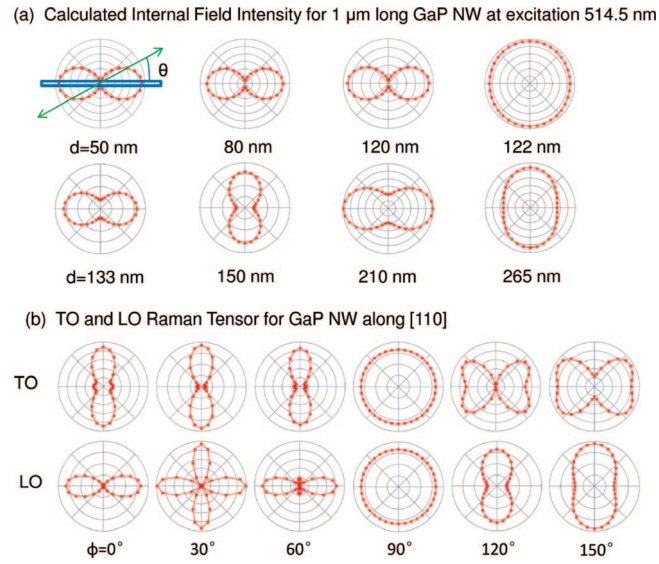

Figure 4. (a) Polarization angle (θ) dependence of the calculated internal EM intensity $\bar{I}_{Int}(\theta)$ (DDA) for $L = 1$ μm GaP NW for several diameters in the range $50 < d < 265$ nm using 514 nm excitation. (b) Calculated θ-dependence of the contribution to the Raman scattering from the Raman tensor (eq 1). Calculations are for a ⟨110⟩ GaP NW oriented along the x-axis (Figure 1) and shown for various angles φ between the ⟨1$\bar{1}$2⟩ NW direction and the z-axis.

that these values of d are near resonance peaks for $L = 1$ μm wires, such as shown for $L = 2$ μm wires in Figure 2c. As can be seen in Figure 4a, for $d = 122-265$ nm, the θ-dependence of the average internal field intensity is much more isotropic (almost perfectly isotropic for $d = 122$ nm) and the most efficient polar angle for inducing a strong internal field alternates in this range of d between TE and TM excitation. The large change in the polar plots between $d = 120$ nm and $d = 122$ nm indicates that $\bar{I}_{int}$ ($\sim Q_i^2$) can be very sensitive to diameter as evidenced in Figure 2c.

In Figure 4b, for the case of a ⟨110⟩ growth axis, we display the θ-dependence of the factor in eq 1 containing the Raman tensor, i.e., $|\hat{e}_i \cdot R \cdot \hat{e}_s|^2$ for $\hat{e}_i||\hat{e}_s$ and for several angles φ between the ⟨1$\bar{1}$2⟩ direction and the laboratory z-axis (Figure 1a). As can be seen in the figure, since the form of R depends on the type of phonon scattered, the polar plots for TO and LO scattering can be different. The varieties of patterns seen in the figure indicate the sensitivity of the scattering pattern to the NW orientation. As indicated in eq 1, the polar plot for TO and LO Raman scattering is proportional to the product of the two factors $Q^4 \sim (I_{int}^2/I_i^2)$ and $|\hat{e}_0 \cdot R \cdot \hat{e}_s|^2$.

In Figure 5, we display the experimental polarized Raman scattering patterns $I_s(\theta)$ for LO and TO backscattering collected on various individual GaP NWs using 514.5 nm excitation. Data in the figure (dots) are taken on wires either suspended over a hole in a TEM grid (cf. $d = 80$ nm, 133 nm) or supported on a Si substrate ($d = 50$, 265, 265 nm). As already discussed, for wires on a TEM grid, the TEM image and SAD pattern were used to determine the wire diameter and the growth axis; for NWs on Si substrates, AFM z-scan was used to measure the diameter and the growth direction is not known. The data are plotted as dots and the

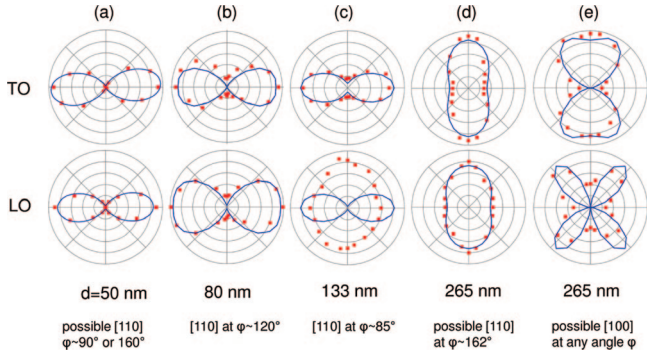

Figure 5. Experimental polar (θ) plots (dots) of the TO (upper) and LO (lower) polarized Raman backscattering from individual GaP NWs collected with 514.5 nm excitation. Solid curves calculated according to eq 1. Column (a) $d = 50$ nm wire on Si, column (b) $d = 80$ nm wire on a TEM grid, column (c) $d = 133$ nm on a TEM grid, column (d) $d = 265$ nm on Si, and column (e) $d = 265$ nm on Si. The labels found below the diameter values indicate the growth axis and tipping angle φ used in the calculations.

curves are calculated on the basis of eq 1 using the DDA to compute $Q^4 \sim (\bar{I}_{int}/I_i)^2$ for a $L = 1$ μm NW. In Figure 5a, we show the results for a $d = 50$ nm wire with unknown growth axis supported on a Si substrate. The LO and TO Raman scattering patterns are dominated by the Q^4 factor and it is therefore difficult to determine the growth axis and φ that stem from the Raman tensor factor. However, we present the calculated result for the TO and LO patterns for $d = 50$ nm, $\langle 110 \rangle$ growth axis, $\varphi \approx 90°$ or 160°. The TO and LO patterns both exhibit $\sim\cos^4(\theta)$ dependence. For two NWs on TEM grids, we know the $\langle hkl \rangle$ growth axis from SAD. These wires have $d = 80$ and 133 nm NW and they both grew along $\langle 110 \rangle$. Both the experimental TO and LO patterns of a $d = 80$ nm wire (Figure 5b) can be described as an "open dipole" (i.e., the patterns are dipole-like and open at the origin); the solid curve is for a $\langle 110 \rangle$ wire with $\varphi = 120°$. For the $d = 133$ nm $\langle 110 \rangle$ NW (Figure 5c) the experimental TO pattern is also an "open dipole", while the experimental LO pattern is nearly elliptical and with a relative rotation of 90° with respect to the TO pattern. Our best model calculation (the solid curve is for a $\langle 110 \rangle$ wire with $\varphi = 85°$) has trouble with the LO pattern. The model predicts weak LO scattering for $\theta = 90°$. Finally, for two $d = 265$ nm NWs supported on Si, we observe two distinct pairs of experimental polar scattering patterns. The difference can be identified with different growth directions, $\langle 110 \rangle$ (Figure 5d) and $\langle 110 \rangle$ (Figure 5e). The former direction produces nearly elliptical LO and TO patterns, both oriented along $\theta = 90°$ for $\varphi \sim 162°$. The $\langle 100 \rangle$ NW, on the other hand, produces a "quadrupole-like" LO pattern and a rotated and distorted "dipolar-like" pattern for the TO scattering. For NWs that grew along $\langle 100 \rangle$ we lose information about φ because the calculated Raman tensor polar patterns for both TO and LO phonons are independent of the angle φ. This is a special consequence of the symmetry of the LO and TO phonon displacement relative to the lattice and is predicted by group theory.[26]

Summary and Conclusions. We have shown that polarized LO and TO Raman scattering from GaP NWs presents a wide variety of patterns which stem from the interplay of photon confinement, the NW growth direction, and the orientation of the NW crystallographic axes with respect to the incident electric field. For small diameter GaP wires ($d < 65$ nm), the polar scattering patterns are dominated by an optical antenna effect and a simple $\cos^4(\theta)$ pattern is observed. This "antenna effect" should be a general result for any SNWs where the optical loss is not too high. As the diameter of the GaP NW increases, higher order volume antennae effects are observed in which TM excitation is much more efficient than TE excitation in establishing the internal EM fields. It is clear that the weak link in our current understanding of the experimental data is in the quantitative aspects of the confined polarized photon states. More sophisticated calculations are needed to predict the internal electromagnetic fields. In particular, they should be constructed to handle the case of long wires that are centrally illuminated in a focal spot whose diameter is much less than their length.

Acknowledgment. The financial support for this work (P.C.E., Q.X., G.C., J.W.) was provided by NSF-NIRT (Nanotechnology and Interdisciplinary Research Initiative), Grant DMR-0304178. This work was supported in part (D.H.W., M.E.P., J.S.P.) by the Penn State Materials Research Institute and the Penn State MRSEC under NSF Grant No. DMR 0213623. We thank Dr. Kevin Shuford (ORNL) for assistance with the DDA code.

References

(1) Slepyan, G. Y.; Shuba, M. V.; Maksimenko, S. A.; Lakhtakia, A. *Phys. Rev. B* **2006**, *73* (19), 195416.
(2) Balanis, C. A. *Advanced Engineering Electromagnetics*; Wiley: New York, 1989.
(3) Ajiki, H.; Ando, T. *Physica B* **1996**, *216* (3–4), 358–361.
(4) Duesberg, G. S.; Loa, I.; Burghard, M.; Syassen, K.; Roth, S. *Phys. Rev. Lett.* **2000**, *85* (25), 5436–5439.
(5) Saito, R.; Jorio, A.; Hafner, J. H.; Lieber, C. M.; Hunter, M.; McClure, T.; Dresselhaus, G.; Dresselhaus, M. S. *Phys. Rev. B* **2001**, *64*, 085312.
(6) Jorio, A.; Souza, A. G.; Brar, V. W.; Swan, A. K.; Unlu, M. S.; Goldberg, B. B.; Righi, A.; Hafner, J. H.; Lieber, C. M.; Saito, R.; Dresselhaus, G.; Dresselhaus, M. S. *Phys. Rev. B* **2002**, *65* (12), 121402.
(7) Wang, Y.; Kempa, K.; Kimball, B.; Carlson, J. B.; Benham, G.; Li, W. Z.; Kempa, T.; Rybczynski, J.; Herczynski, A.; Ren, Z. F. *Appl. Phys. Lett.* **2004**, *85* (13), 2607–2609.
(8) Rafailov, P. M.; Thomsen, C.; Gartsman, K.; Kaplan-Ashiri, I.; Tenne, R. *Phys. Rev. B* **2005**, (20), 72.
(9) Livneh, T.; Zhang, J. P.; Cheng, G. S.; Moskovits, M. *Phys. Rev. B* **2006**, (3), 74.
(10) Pauzauskie, P. J.; Talaga, D.; Seo, K.; Yang, P. D.; Lagugne-Labarthet, F. *J. Am. Chem. Soc.* **2005**, *127* (49), 17146–17147.
(11) Frechette, J.; Carraro, C. *Phys. Rev. B* **2006**, (16), 74.
(12) Xiong, Q. H.; Gupta, R.; Adu, K. W.; Dickey, E. C.; Lian, G. D.; Tham, D.; Fischer, J. E.; Eklund, P. C. *J. Nanosci. Nanotechnol.* **2003**, *3* (4), 335–339.
(13) Gupta, R.; Xiong, Q.; Mahan, G. D.; Eklund, P. C. *Nano Lett.* **2003**, *3* (12), 1745–1750.
(14) Barker, A. S. *Phys. Rev.* **1968**, *165* (3), 917.
(15) Xiong, Q. H.; Wang, J. G.; Reese, O.; Voon, L.; Eklund, P. C. *Nano Lett.* **2004**, *4* (10), 1991–1996.
(16) Rayleigh, L. *Philos. Mag.* **1918**, *36* (215), 365.
(17) Kerker, M. *The Scattering of Light, and other Electromagnetic Radiation*; Academic Press: New York, 1969.
(18) Ruppin, R. *Journal of Optical Society of America A* **1998**, *15* (7), 1891–1895.

(19) Cao, L. Y.; Nabet, B.; Spanier, J. E. *Phys. Rev. Lett.* **2006**, (15), 96.
(20) Draine, B. T.; Flatau, P. J. *J. Opt. Soc. Am. A* **1994**, *11* (4), 1491–1499.
(21) Draine, B. T.; Flatau, P. J. *User Guide for the Discrete Dipole Approximation code DDSCAT6.1*, http://arxiv.org/abs/astro-ph/0409262, 2006.
(22) Loudon, R. *Adv. Phys.* **2001**, *50* (7), 813–864.
(23) *Light Scattering in Solids I: Introductory Concepts*, 2nd corr. and updated ed.; Cardona, M., Brodsky, M. H., Eds.; Topics in Applied Physics; Springer-Verlag: Berlin, NY, 1983.
(24) *Light Scattering in Solids IX: Novel Materials and Techniques*; Cardona, M., Merlin, R., Eds.; Topics in Applied Physics; Springer-Verlag: Berlin, NY, 2007.
(25) Yu, P. Y.; Cardona, M. *Fundamentals of semiconductors: physics and materials properties*, 2nd updated edition; Springer-Verlag: Berlin, NY, 1999.
(26) The details of the Raman tensor calculations will be discussed in a long paper that will be submitted for publication.

NL080007V